Journal Pre-proof

Electrochemical nitrate removal by magnetically immobilized nZVI anode on ammonia-oxidizing plate of RuO$_2$–IrO$_2$/Ti

Xiaoting Hong, Yingying Du, Haibin Zhang, Wenjuan Xue, Kwan San Hui, Gangming Fang

Please cite this article as: Hong, X., Du, Y., Zhang, H., Xue, W., San Hui, K., Fang, G., Electrochemical nitrate removal by magnetically immobilized nZVI anode on ammonia-oxidizing plate of RuO$_2$–IrO$_2$/Ti, *Chemosphere* (2022), doi: https://doi.org/10.1016/j.chemosphere.2022.133806.

This is a PDF file of an article that has undergone enhancements after acceptance, such as the addition of a cover page and metadata, and formatting for readability, but it is not yet the definitive version of record. This version will undergo additional copyediting, typesetting and review before it is published in its final form, but we are providing this version to give early visibility of the article. Please note that, during the production process, errors may be discovered which could affect the content, and all legal disclaimers that apply to the journal pertain.

Author contributions statement

Xiaoting Hong, Yingying Du, Haibin Zhang, Wenjuan Xue contributed to the conception of the study;

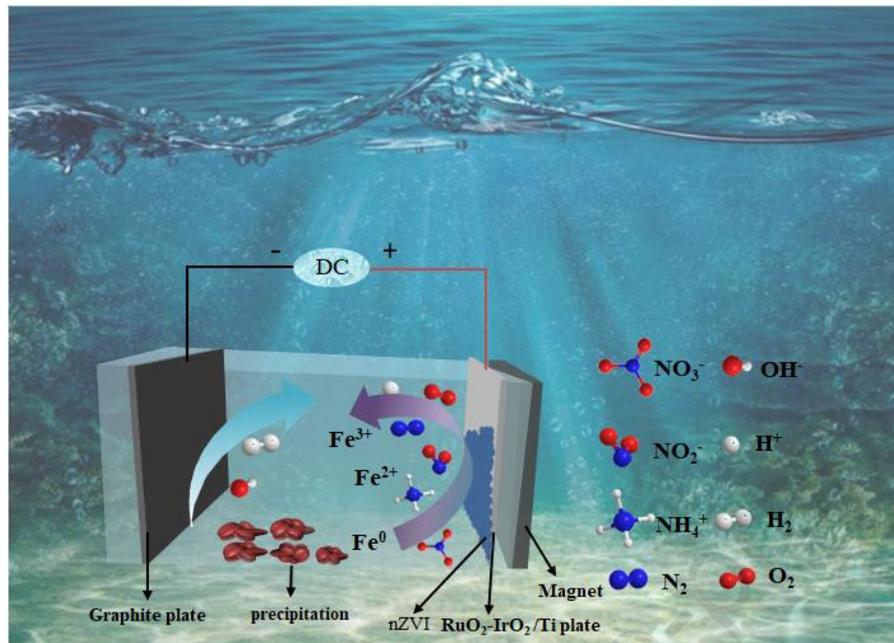Yingying Du, Wenjuan Xue performed the experiment;

Xiaoting Hong, Yingying Du contributed significantly to analysis and manuscript preparation;

Xiaoting Hong, Yingying Du performed the data analyses and wrote the manuscript;

Kwan San Hui, Gangming Fang helped perform the analysis with constructive discussions;

Xiaoting Hong, Yingying Du, and Haibin Zhang contributed to the revision of the manuscript.

Graphical abstract

1 **Electrochemical nitrate removal by magnetically immobilized nZVI anode on**

2 **ammonia-oxidizing plate of RuO$_2$-IrO$_2$/Ti**

3

4 Xiaoting Hong [a,*,†], Yingying Du [a,†], Haibin Zhang [b], Wenjuan Xue [a], Kwan San Hui [c],

5 Gangming Fang [d]

6

7 [a] Department of Chemistry, Zhejiang Sci-tech University, Hangzhou 310018, P.R.

8 China

9 [b] Zhejiang Ruicheng New Materials Co., Ltd, Wenzhou 325401, P.R. China

10 [c] Engineering, Faculty of Science, University of East Anglia, Norwich, NR4 7TJ,

11 United Kingdom

12 [d] Hangzhou Chuan En Environmental Technology Co., LTD, Hangzhou 311508, P.R.

13 China

14

15

16

17

18 [†] These authors contributed equally to this study.

19 Corresponding author. Tel.: +86 (0571) 86843228, Fax +86 (0571) 86843228.

20 E-mail address: hanren.xiaoting@gmail.com (X.T. Hong).

21

22

Abstract

Ammonium as the major reduction intermediate has always been the limitation of nitrate reduction by cathodic reduction or nano zero-valent iron (nZVI). In this work, we report the electrochemical nitrate removal by magnetically immobilized nZVI anode on RuO_2-IrO_2/Ti plate with ammonia-oxidizing function. This system shows maximum nitrate removal efficiency of 94.6 % and nitrogen selectivity up to 72.8 % at pH of 3.0, and it has also high nitrate removal efficiency (90.2 %) and nitrogen selectivity (70.6 %) near neutral medium (pH=6). As the increase of the applied anodic potentials, both nitrate removal efficiency (from 27.2 % to 94.6 %) and nitrogen selectivity (70.4 % to 72.8 %) increase. The incorpration of RuO_2-IrO_2/Ti plate with ammonia-oxidizing function on the nZVI anode enhances the nitrate reduction. The dosage of nZVI on RuO_2-IrO_2/Ti plate (from 0.2 g to 0.6 g) has a slight effect (the variance is no more than 10.0 %) on the removal performance. Cyclic voltammetry, Tafel analysis and electrochemical impedance spectroscopy (EIS) were further used to investigate the reaction mechanisms occurring on the nZVI surfaces in terms of CV curve area, corrosion voltage, corrosion current density and charge-transfer resistance. In conclusion, high nitrate removal performance of magnetically immobilized nZVI anode coupled with RuO_2-IrO_2/Ti plate may guide the design of improved electrochemical reduction by nZVI-based anode for practical nitrate remediation.

Keywords: nanoscale zero-valent iron (nZVI); electrochemical removal; N_2 selectivity; nitrate;

1. Introduction

Excessive application of nitrogen fertilizers and substantial discharge of treated or accidental leakage of untreated wastewater have led to an increase in nitrate concentrations in water bodies and become a common environmental problem (Zhang et al., 2018; Aggrwal et al., 2021; Ma et al., 2021). Nitrate is easily converted to nitrite by microorganisms in the human body, and nitrite can oxidize low-iron hemoglobin, which normally carries oxygen in the blood, to methemoglobin, thus losing its oxygen-carrying capacity and causing tissue hypoxia, making it difficult to breathe and causing acute poisoning and damage to the nervous system (Wei et al., 2018; Singh et al., 2022). In addition, nitrite reacts with secondary amines to form substances that are carcinogenic and teratogenic to humans (Yang et al., 2018). It is therefore becoming increasingly important to raise awareness of the existence of these health hazards issues indirectly caused by nitrates. The World Health Organization (WHO) has set a limit of 11.3 mg L^{-1} for NO_3^--N in drinking water (Puggioni et al., 2021).

In recent years, environmental scientists have conducted numerous studies on the remediation technology of nitrate pollution. There are three main types of nitrate pollution remediation techniques including physicochemical remediation, bioremediation, and chemical reduction according to their principles (Fan et al., 2021; Liu et al., 2021; Pang and Wang, 2021). The physicochemical methods mainly include distillation, electrodialysis, reverse osmosis, ion exchange with high cost and ordinary efficiency. Biological remediation is the use of denitrifying bacteria to transform

67   nitrate into nitrogen, but this technique is generally limited to areas with good

68   geological conditions and small contaminated areas. Chemical reduction remediation

69   is a fast and effective remediation method that uses certain reducing agents to reduce

70   the nitrate in the water (Ramalingam and Subramania, 2021). Zero-valent iron (ZVI)

71   has attracted great attention for an excellent alternative (Liu and Wang, 2019).

72   Especially, nano zero-valent iron (nZVI) has become one of the most widely used

73   reducing agents due to its higher reactivity and better removal efficiency (Khalil et al.,

74   2018).

75   Various researches have been conducted to optimize the reaction conditions

76   (dosage, temperature, current densities, co-existing ions, etc.) (Guo et al., 2020),

77   synergistic reaction with other reagents such as persulfate (Wang et al., 2021b),

78   intermediate products (Zhang et al., 2017), nZVI based-composites (Jiang et al., 2012;

79   Qi et al., 2021; Wu et al., 2021), and doped nZVI (Su et al., 2014), etc. for nitrate

80   reduction. Among these reduction reactions the most difficulty is to steadily enhance

81   the N_2 selectivity and elucidate the reaction mechanisms and pathways. Recently, one

82   of the nitrate reduction research directions under external stimuli of an applied

83   electrical field has gained strong interest. Most conventionally, electrocoagulation

84   (EC) or a combination of EC and electrooxidation (EO) was studied as a

85   denitrification process to efficiently remove nitrate by iron or aluminum plate anodes

86   (Amarine et al., 2020; Benekos et al., 2021). Ti/RuO$_2$ anode was combined to enhance

87   the N_2 selectivity and removal efficiency of iron EC system for the treatment of actual

88   wastewater containing high concentration of nitrate ion based on the anodic ammonia

89 oxidation (Chauhan and Srivastava, 2020; Li et al., 2021; Pellessier et al., 2021).

90 Novel nZVI nanostructures were also explored to achieve high nitrate removal

91 efficiency and N_2 selectivity by electrocatalytic denitrification (Wang et al., 2021a).

92 All of the above-mentioned electrocatalytic researches were about cathodic nitrate

93 reduction. However, nZVI related electrocatalytic denitrification via anodic nitrate

94 reduction is rarely reported.

95   In this study, nZVI-related composite anodes constructed on RuO_2-IrO_2/Ti

96 electrode (nZVI/ RuO_2-IrO_2/Ti) by magnetic force immobilization were used to

97 explore the synergistic effects of intrinsic reduction property of nZVI, anodic current,

98 ammoxidation characteristic of RuO_2-IrO_2/Ti, and nZVI electro-coagulation on the

99 nitrate removal. Electrochemical denitrification activity and N_2 selectivity was

100 evaluated under different reaction parameters such as the combination of the

101 composite anode, nZVI dosage, initial solution pH, background electrolyte, applied

102 voltage, and initial nitrate concentration. The underlying reaction mechanisms of

103 electrocatalytic denitrification were proposed. The final results showed that the

104 experimental system is of great significance for denitrification treatment of water with

105 high performance about nitrate removal efficiency and N_2 Selectivity.

106

107 **2   Materials and methods**
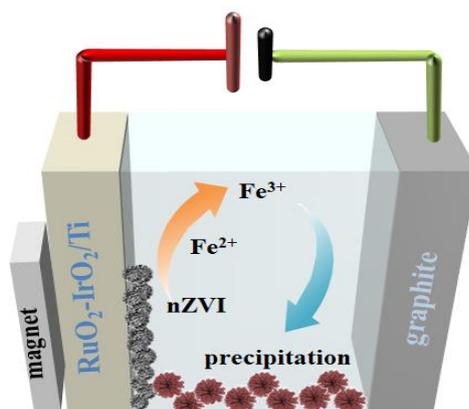
108 2.1 Materials and reagents

109   The pH of aqueous solution was adjusted by 3 M of NaOH or 1 M of H_2SO_4 in

110 each experiment. The conductivity of aqueous solution was adjusted by 500 mg L^{-1} of

111 Na$_2$SO$_4$. Furthermore, nZVI was purchased from Shanghai Xiangtian Nano Material

112 Co., Ltd. RuO$_2$-IrO$_2$/Ti plate and graphite sheet were supplied by Suzhou Shude

113 Industrial Machinery Co., Ltd. Nitrate solution was prepared with ultrapure water

114 using NaNO$_3$.

115

116 2.2 Experimental setup

117 Electrochemical denitrification experiments were carried out in 500 mL glass

118 jars. Different initial concentrations (50, 100 and 500 mg L^{-1}) of nitrate solution with

119 a volume of 400 mL were prepared using sodium nitrate. Different concentrations of

120 Na$_2$SO$_4$ (0, 250, 500 mg L^{-1}) were used as the background electrolyte. The area of

121 RuO$_2$-IrO$_2$/Ti plate immersed in the solution was ~ 45 cm^2. A certain amount of nZVI

122 powder was uniformly distributed on the RuO$_2$-IrO$_2$/Ti plate with a dimension of 16.5

123 × 3.0 cm^2. The nZVI powders were fixed to the RuO$_2$-IrO$_2$/Ti plate surface by a 2.8

124 cm × 7.8 cm × 0.4 cm magnet labeled as nZVI-RuO$_2$-IrO$_2$/Ti composite anode. An

125 nZVI-graphite composite anode was also prepared using same method with a graphite

126 plate. A pure graphite cathode was connected in parallel to the anode at a distance of

127 1.5 cm under different applied voltages. The experimental setup is shown in Fig. 1.

128

129   **Fig. 1** Schematic diagram of the experimental setup.

130

131   2.3 Experimental methods

132   Many factors affecting nitrate removal were investigated, including anode

133   material, applied voltage, initial pH, nano-zero-valent iron dose, electrolyte

134   concentration, initial nitrate concentration. The nZVI-RuO$_2$-IrO$_2$/Ti, mZVI-

135   RuO$_2$-IrO$_2$/Ti, iron filings-RuO$_2$-IrO$_2$/Ti, RuO$_2$-IrO$_2$/Ti, and nZVI-graphite were used

136   as the anodes in this study. The effects of various applied voltages of 1.2 V, 3.0 V, 5.0

137   V, 10.0 V and initial pH values of 3, 6, 10 on the nitrate removal were studied.

138   Different electrolytes of FeSO$_4$, FeCl$_2$ and Na$_3$PO$_4$ (500 mg L^{-1}) were also used to

139   explore their effects on nitrate removal compared to Na$_2$SO$_4$. Each experiment was

140   conducted for 5 h with a sampling interval of 0.5 h and thereafter each sample was

141   filtered through a membrane filter (pore size of 0.45 μm) before testing. The

142   concentrations of nitrate, nitrite and ammonium were determined by ion

143   chromatography (Eco-IC, Metrohm). Iron ions were analyzed spectrophotometrically

144   by forming the reddish-orange tris complex of iron (II) and 1,10-phenanthroline. The

145   pH and conductivity of the solution were measured by pH meter (FiveEasy,

146   METTLER TOLEDO).

147   The percentage of nitrate removal ($R_{NO_3^-}$), N$_2$ selectivity (S_{N_2}) of the

148   electrochemical denitrification were calculated using the following equations (Wang

149   et al., 2021a):

150
$$R_{NO_3^-} = \frac{[\text{NO}_3^-]_0 - [\text{NO}_3^-]_f}{[\text{NO}_3^-]_0} \times 100\%$$
Eq. (1)

7

151
$$S_{N_2} = \frac{[NO_3^-]_0 - [NO_3^-]_f - [NO_2^-]_f - [NH_4^+]_f}{[NO_3^-]_0 - [NO_3^-]_f} \times 100\%$$

Eq. (2)

152   The subscripts of 0 and f in the equation represent the initial and final

153   concentrations (mg L^{-1}) of NO_3^-, NO_2^-, and NH_4^+, respectively. All samples were

154   analyzed at least in triplicate.

155

156   2.4 Characterization techniques

157   The final precipitate of the reaction as well as the residual nZVI were collected,

158   filtered, and then dried at 80°C under vacuum. X-ray powder diffraction (XRD)

159   patterns of the resultant precipitate and nZVI (before and after reaction) were

160   recorded using the DX-2700 (Dandong Haoyuan Instrument) diffractometer with

161   monochromatic Cu Ka irradiation in the 2θ angular regions between 10 ° and 80 °. The

162   surface morphology, atomic composition and distribution of the precipitate were

163   measured by scanning electron microscopy equipped with a dispersive X-ray

164   spectroscopy detector (SEM/EDS, Inspect F50, FEI). Different valence states of Fe

165   and oxygen in final precipitate were measured by X-ray photoelectron spectroscopy

166   (XPS) (K-Alpha, Thermo Fisher Scientific). The split-peak fitting operations were

167   performed by XPSPEAK41 software. Tafel analysis, cyclic voltammetry (CV), and

168   electrochemical impedance spectroscopy (EIS) were used to strengthen the

169   mechanism interpretation by an electrochemical workstation (Chenhua, CHI 660A,

170   Shanghai). Tafel curves were measured at nitrate solution with an initial concentration

171   of 100 mg L^{-1} and 0.6 g of nZVI. EIS diagram was carried out at an initial voltage of

172   -0.3 V with high frequency of 10^5 and low frequencies of 10^{-2}. Cyclic voltammetry

173   curves were obtained at a scanning rate of 100 mV s^{-1} between -1.8 and 1.8 V (versus
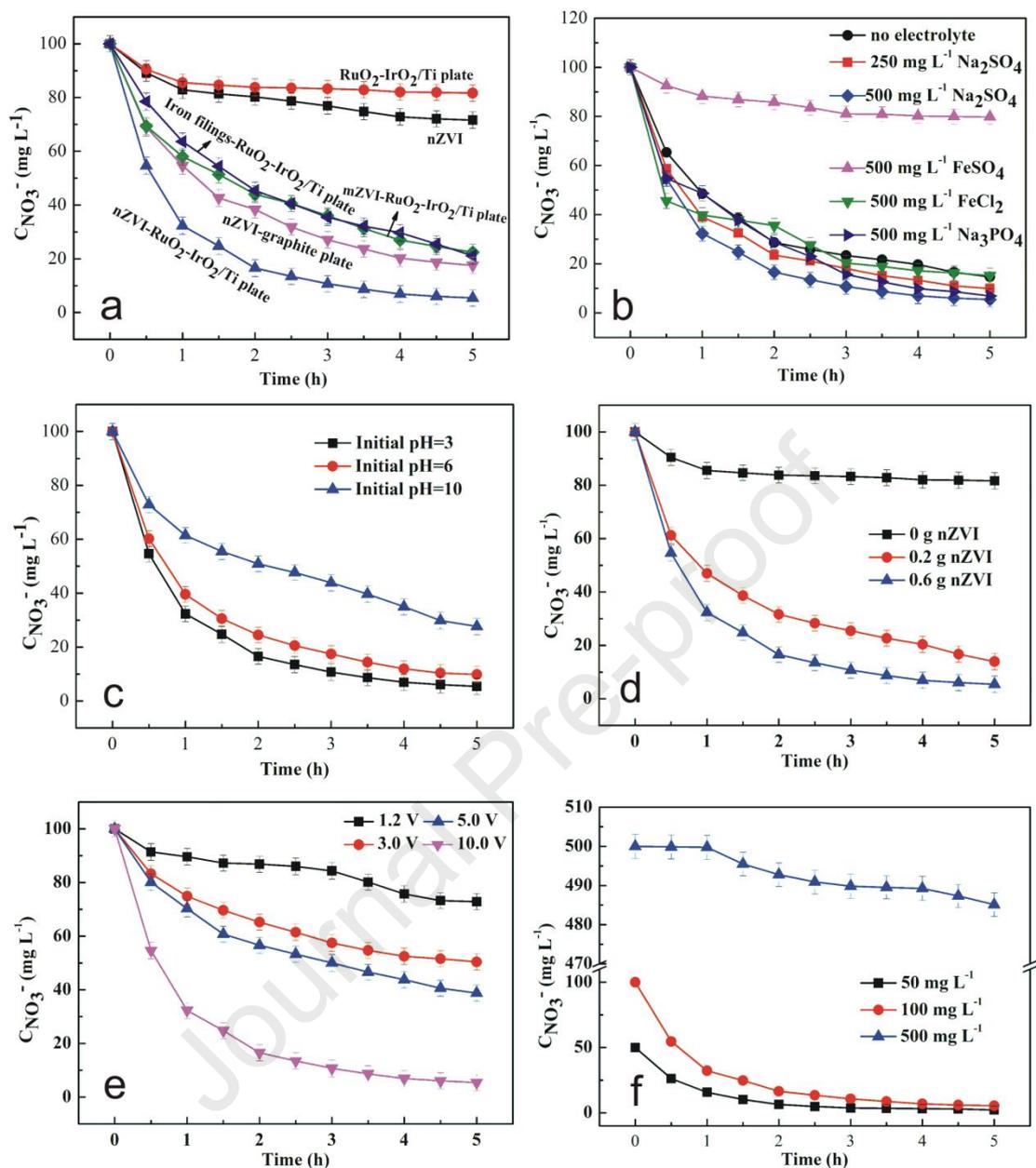
174   Ag/AgCl).

175

176   **2. Results and discussion**

177   3.1 Effect of different reaction parameters on electrochemical denitrification

178   3.1.1   Anode materials

179   The comparative NO_3^- reduction efficiency on different anodes such as

180   nZVI-RuO$_2$-IrO$_2$/Ti, mZVI-RuO$_2$-IrO$_2$/Ti, iron filings-RuO$_2$-IrO$_2$/Ti, RuO$_2$-IrO$_2$/Ti

181   and nZVI-graphite was depicted in Fig. 2a. Additionally, direct spreading nZVI into

182   nitrate solution without electric field was also investigated to compare the

183   denitrification result. Obviously, the nitrate removal efficiency on nZVI-RuO$_2$-IrO$_2$/Ti

184   anode was significantly higer than that in single RuO$_2$-IrO$_2$/Ti or nZVI system. The

185   NO_3^- concentration was finally reduced to 5.42 mg L^{-1} and the removal rate reached

186   94.6 % on nZVI-RuO$_2$-IrO$_2$/Ti anode after 5 h under the conditions of initial nitrate

187   concentration of 100 mg L^{-1}, voltage of 10V, temperature of 25 °C, pH of 3,

188   electrolyte concentration of 500 mg L^{-1} Na$_2$SO$_4$ and nZVI dosage of 0.6g. In contrast,

189   the nitrate removal rates of RuO$_2$-IrO$_2$/Ti anode and nZVI alone under the same

190   reaction conditions were only 18.3 % and 28.4 %, respectively. Either nZVI or

191   RuO$_2$-IrO$_2$/Ti on nZVI-RuO$_2$-IrO$_2$/Ti was repalced by mZVI and iron fillings or

192   graphite, the removal rate was decreased to 77.6 %, 78.9 %, and 82.4 %, respectively.

193

Fig. 2 Influence of different factors on nitrate removal, a) anode materials, b) electrolyte concentrations, c) initial pH, d) dose of nZVI, e) applied voltages, f) initial nitrate concentrations.

197

As indicated on Fig. 3a, the main intermediate of electrochemical nitrate reduction on these different electrodes is NH_4^+ and the toxic intermediate NO_2^- was negligibly detected in all cases. The anode composition has a very important influence on the

10

201 intermediate and the N_2 selectivity. Correspondingly, nitrate reduction on

202 nZVI-RuO$_2$-IrO$_2$/Ti electrode has a higher value of N_2 selectivity (72.8 %) than other

203 electrodes (e.g., 63.8 % for nZVI-graphite electrode), which is compareble to previous

204 result (74.0 %) conducted on ordered mesoporous carbon nZVI cathode elsewhere

205 (Teng et al., 2018).

206

207 3.1.2 Electrolyte concentration

208 Fig. 2b shows the effect of different electrolyte concentrations on nitrate removal

209 for nZVI-RuO$_2$-IrO$_2$/Ti electrode. Initially, the nitrate removal rate was 85.3 %

210 without addition of Na$_2$SO$_4$. The gradual increase of the removal rate to 90.12% and

211 94.6 % was observed for the systems with 250 and 500 mg L^{-1} Na$_2$SO$_4$, respectively.

212 Similar trends were observed for the value of N_2 selectivity which increases from

213 68.3 % to 70.9 % and 72.8 % with the increase the electrolyte concentration from 0

214 mg L^{-1} to 250 and 500 mg L^{-1}, respectively (Fig. 3b). Obviously, increasing the

215 electrolyte concentration could not only enhance the nitrate removal rate, but also

216 improve the N_2 selectivity. Higher concentration of supporting electrolyte leads to

217 stronger anodic dissolution, thus protecting the nZVI particles from passivation
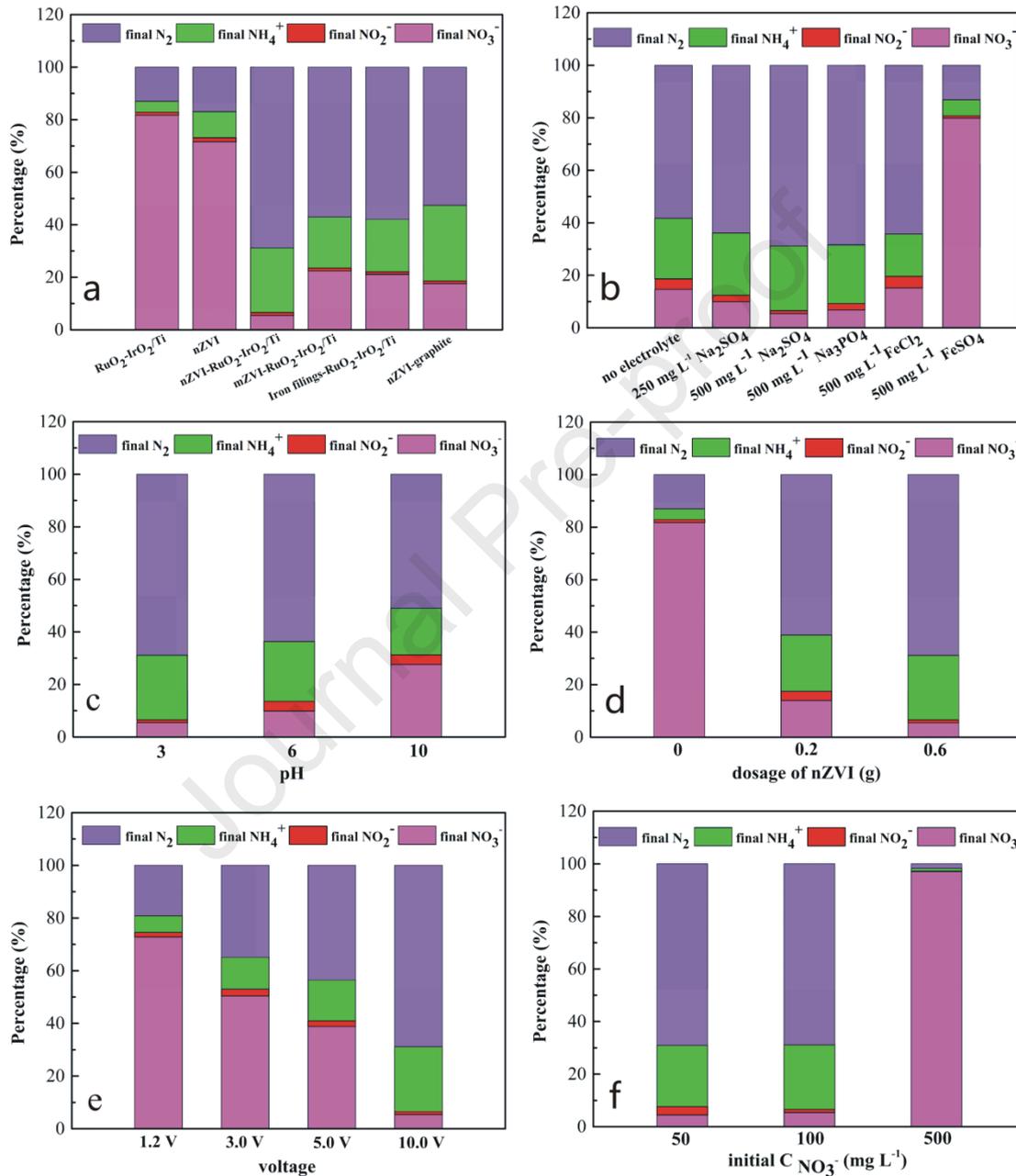
218 (Katsounaros and Kyriacou, 2007).

219 Three different background electrolyte of FeSO$_4$, FeCl$_2$ and Na$_3$PO$_4$ with 500 mg

220 L^{-1} were used to investigate the effect of Fe^{2+}, Cl$^-$ and PO$_4^{3-}$ on the nitrate removal

221 efficiency. Unexpectedly, subtituting Na$_2$SO$_4$ with FeSO$_4$ dramatically reduced the

222 nitrate removal efficiency from 94.6 % to 20.2 %. Although surface-bound Fe^{2+} may

11

223   enhance the electron transfer from the nZVI core to the solid–liquid interface, and

224   thus improve the performance of the nitrate reduction by nZVI (Huang and Zhang,

225   2005). However, nZVI was bound on the anodes in this study and positive charged

226   Fe^{2+} were hard to surface bound due to its preference to migrate to the cathode surface.

227   Further replacing Na_2SO_4 with other iron electrolyte of $FeCl_2$, the nitrate removal

228   efficiency was partially recovered to 84.8 %. The presence of chloride ions could

229   significantly accelerate the reaction rate for NH_4^+ oxidation on supporting anode of

230   RuO_2-IrO_2/Ti and subsequently the nitrate reduction reaction moves forward direction

231   (Sun et al., 2020; Song et al., 2021). Apparently, the nitrate removal efficiency in

232   Na_3PO_4 (93.2 %) was very close to that of Na_2SO_4 system (94.6 %).

233   3.1.3   Initial pH

234   The effect of various initial pH values (3.0, 6.0, and 11.0) of electrolyte on the

235   electrocatalytic nitrate reduction of nZVI-RuO_2-IrO_2/Ti was performed under the

236   same initial conductivity. A drop from pH 11.0 to 3.0 enhanced both the nitrate

237   removal efficiency from 72.4 % to 94.6 % (Fig. 2c) and N_2 selectivity from 70.5 to

238   72.8 % (Fig. 3c). Nitrate reduction is a protons consumption process ($4Fe^0 + NO_3^- +$

239    $10H^+ \rightarrow 4Fe^{2+} + NH_4^+ + 3H_2O$ $\Delta G= -997.71$ (Alowitz and Scherer, 2002), $2NO_3^-$

240    $+ 12H^+ + 10\ e^- \rightarrow N_2 + 6H_2O$ (Li et al., 2016)), thus acidic condition is more

241   favorable for high nitrate removal rate and N_2 selectivity by coupling the protons and

242   electrons. As each reaction proceeds, the slope of the removal rate tends to be more

243   flat because the gradual increase of the background solution pH in all cases is

244   detrimental to the nitrate reduction. The rapid decline in the nitrate removal rate is

attributed to a rapid passivation of the iron surface under alkaline conditions, while

the acidic condition assists in dissolving the surface (hydr)oxides layer, and reveals

more active sites for the electrochemical nitrate removal (Salam et al., 2015).

Fig. 3 Concentrations of NO_3^-, NO_2^- and NH_4^+ ions in solution with different a) anode

materials, b) electrolyte concentrations, c) initial pH, d) dose of nZVI, e) applied

voltages, and f) initial nitrate concentrations.

252 3.1.4 Dosage of nZVI

253   Fig. 2d shows the effect of the dosage of nZVI on nitrate removal. As privously

254 mentioned, the nitrate removal efficiency was only 18.3 % when RuO_2-IrO_2/Ti was

255 used as the anode without nZVI and significantly increased when nZVI coupling with

256 RuO_2-IrO_2/Ti was used as the anode. As the amount of nZVI increased to 0.2 and 0.6

257 g, the removal efficiency dramatically increased to 86.0 % and 94.6 %.

258 Correspondingly, the N_2 selectivity of nZVI/RuO_2-IrO_2/Ti with 0.2 g or 0.6 g nZVI is

259 71.0 % and 72.8 % (Fig. 3d). Obiviously, the adding nZVI improves the nitrate

260 removal efficiency and N_2 selectivity in a way that the higher the amount of nZVI, the

261 higher the removal of nitrate and N_2 selectivity.

262

263 3.1.5 Applied voltage

264   As shown in Fig. 2e, applied voltage has a great influence on the removal of

265 nitrate indicating that higher current densities lead to the faster nitrate removal. In half

266 hour the nitrate residual (92 mg L^{-1}) is only slightly lower than the initial

267 concentration of 100 mg L^{-1} at applied voltage of 1.2 V. The values are gradual

268 decrease to 83 and 80 mg L^{-1} at applied voltage of 3.0 and 5.0 V. In the case of 10.0 V

269 the residual nitrate rapidly fall to 55 mg L^{-1}. The final removal efficiency of nitrate at

270 applied voltages of 1.2 V, 3.0 V, 5.0 V, and 10.0 V were 27.2 %, 49.6 %, 69.1 % and

271 94.6 % after 5 h, respectively. As the increase of applied voltage from 1.2 V to 10.0 V,

272 the N_2 selectivity slightly increases from 70.4 % to 72.8 % (Fig. 3e).

273

274   3.1.6   Initial nitrate concentration

275   The nitrate removal performance were investigated with nitrate electrigated of

276   different concentrations of 50 mg L^{-1}, 100 mg L^{-1} and 500 mg L^{-1}, respectively (Fig.

277   2f). At the conditions of 10.0 V, pH=3, 500 mg L^{-1} Na$_2$SO$_4$, 25°C and 0.6g nZVI, the

278   nitrate removal efficiencies were 95.6 %, 94.6 % and 3.0 % at initial concentrations of

279   50 mg L^{-1}, 100 mg L^{-1} and 500 mg·L^{-1} nitrate respectively. It was clear that the

280   denitrification efficiency was very high for both the initial nitrate concentration of 50

281   mg L^{-1} and 100 mg L^{-1}, but the nitrate removal efficiency fell to 3.0 % when the initial

282   nitrate concentration was as high as 500 mg L^{-1}. Studies have shown that high initial

283   NO$_3^-$ concentrations lower NO$_3^-$ removal efficiencies because more ions are present

284   in the treated water (Salam et al., 2015), therefore, more time is required for their

285   removal (Salam et al., 2015). As can be seen from Fig. 3f, the N$_2$ selectivity of

286   systems with 50 mg L^{-1} and 100 mg L^{-1} nitrate (72.3 and 72.8 %) is also much larger

287   than that of 500 mg L^{-1} nitrate (60.8 %).

288

289   3.2 The iron ions and pH variation with the reaction

290   In this study all electrochemical nitrate reduction reaction finally leads to a

291   higher pH value for background solution. The most representative parameter of

292   applied voltage variation (3.0 V, 5.0 V and 10.0 V) was selected to investigate its

293   effect on background solution pH along with the contact time (Fig. S1a). The

294   background solution pH was sharply increased from 3 to 10 in one hour under an

295   applied voltage of 10.0 V, however, it took 2.0 and 2.5 h to reach ~ 10 (pH value) for

296   3.0 V and 5.0 V systems. Subsequently, all of the background solutions fluctuate near

297   a pH of 10. Understandably, the background solution pH increase rate is positively

298   correlated with the increase of the applied voltage. Both the nitrate reduction reaction

299   and nZVI coagulation (or corrosion) process were very violent at high voltage.

300   Meanwhile, nitrate reduction reaction consumes more protons at higher voltage and

301   stronger coagulation leads to more alkaline flocs in the solution. Therefore, a large

302   amount of OH^- was rapidly produced in the solution resulting in high value pH.
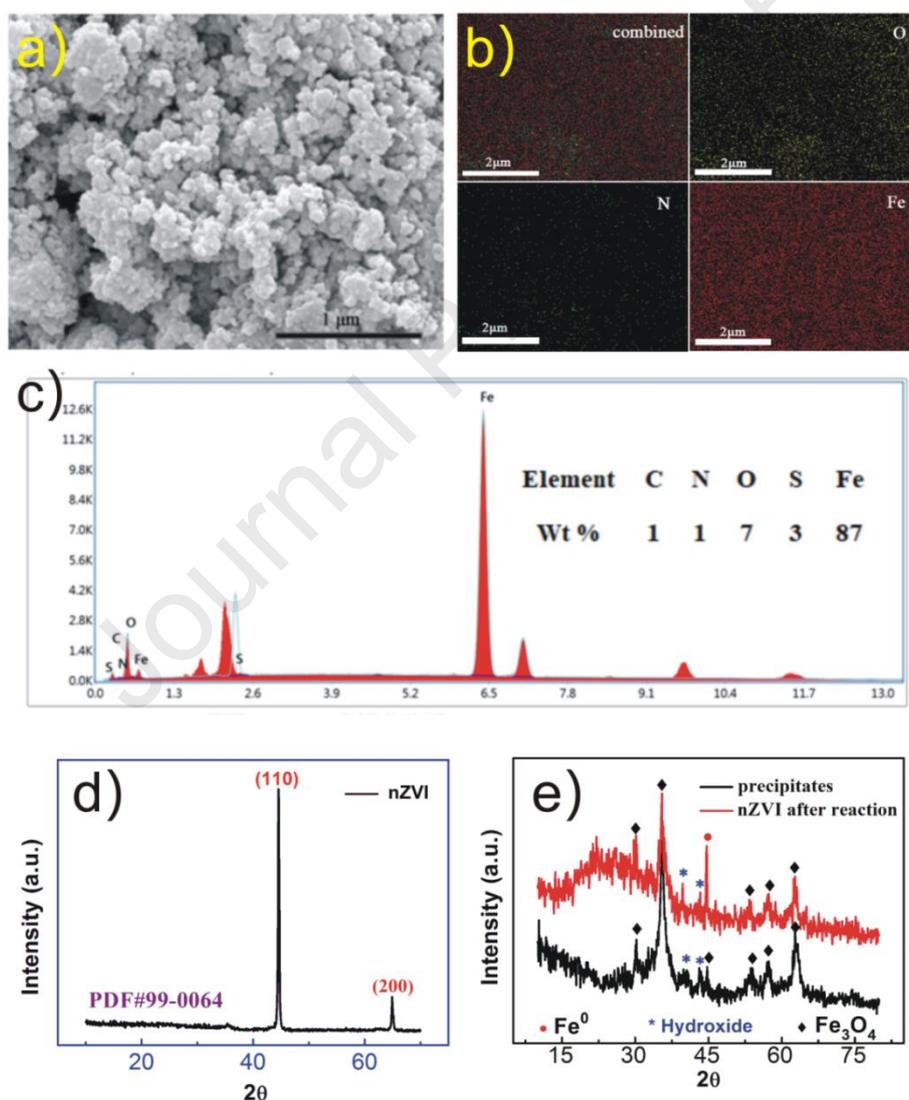
303   Fig. S1b showed the production of ferrous iron and total iron ions in the

304   solution during the nitrate reduction reaction. The concentration of ferrous iron ions

305   rapidly reached 12.8 mg L^{-1} in ten minutes due to violent anodic electro-dissolution,

306   subsequently, the amount of ferrous irons fell sharply to an undetectable value in

307   another fifteen minutes because of fast oxidation by dissolved oxygen from water

308   electrolysis. Then, the presence of ferrous iron ions was no longer detectable in the

309   solution in the rest of the reaction. The total iron content increased persistently in the

310   first four hours of the reaction and decreased slightly in the last hour, probably due to

311   the excessive consumption of nZVI corrosion or greatly enhanced coagulation

312   process.

313

314   3.2 The charateristics of iron-related precipitate

315   The surface morphology and elemental composition of the precipitation were

316   characterized using SEM with an EDS detector. SEM image revealed that the

317   precipitates are of rough and irregular shapes with nanosized domain in an

318   agglomeration state (Fig. 4a). The elemental distributions and elemental compositions

319   of the precipitates were shown in Fig. 4b and Fig. 4c. The elemental mapping images

320   indicated that there are three elements (Fe, O and N) and these elements were evenly

321   distributed on the surface of the precipitates. EDS spectrum showed that the

322   composition of the precipitate contained 87.0 % Fe, 7.0 % O and 1.0 % N element,
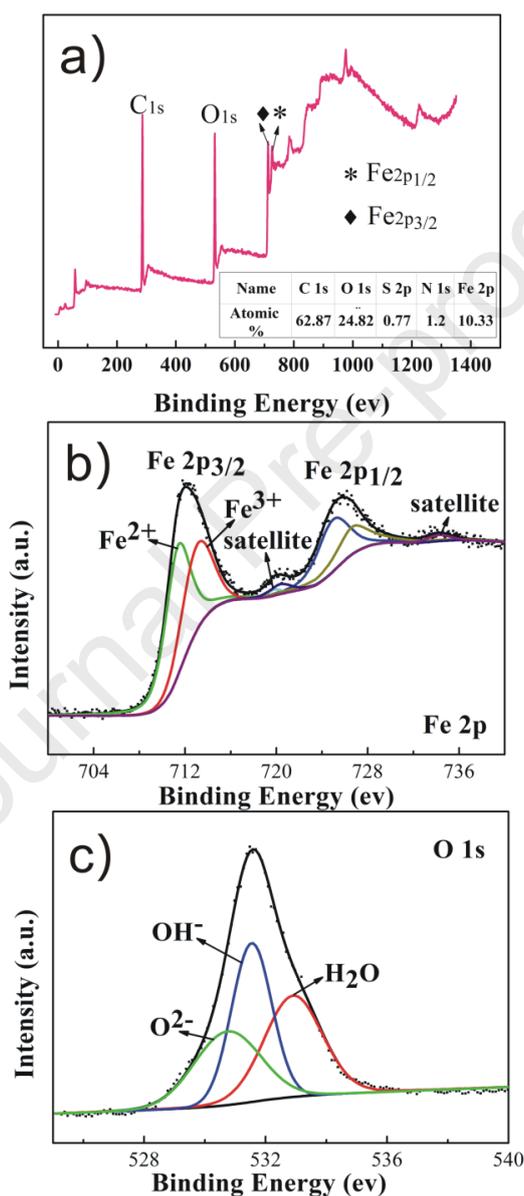
323   respectively.

324

325   **Fig. 4.** a) SEM images, b) elemental mapping of precipitation, c) EDS spectrum of

326   precipitates, and XRD images of d) nZVI before reaction, e) nZVI after reaction and

327   precipitates.

328   XRD patterns of the precipitate, nZVI before and after reaction were displayed in

329   Fig. 4d and Fig. 4e, respectively. The diffraction peaks at 2θ angles of 44.67 ° and

330   64.9 ° accord with peaks of native nZVI (standard card PDF#99-0064) (Su et al.,

331   2019). In addition to the characteristic peak of intrinsic nZVI at 2θ of 44.67 °, the

332   XRD pattern of nZVI after reaction also exhibits peaks at 2θ of 30.07 °, 35.56 °,

333   43.12 °, 44.74 °, 53.65 °, 57. 34 ° and 62.74° that were assigned to the typical

334   characteristics of iron oxides (Fe_3O_4, JCPDS 72-2303) and iron hydroxides (γ-FeOOH,

335   JCPDS 74-1877) (Fig. 4b). The precipitation collected from the reaction solution also

336   exhibited same peaks of iron oxides and iron hydroxides which indicates the fact that

337   part of the precipitate was adhered to the nZVI surface during the reaction (Fig. 4b)

338   (Huang et al., 2020).

339   XPS measurements were also performed to investigate the composition and the

340   chemical state of the precipitate. Fig. 5a shows the XPS spectra of the precipitates

341   revealing the presence of C, Fe, O, N and S in the sample. N and S elements were

342   contributed by the nitrate/intermediates and sulphate electrolyte. The Fe 2p spectrum

343   consisted of Fe $2p_{3/2}$ and Fe $2p_{1/2}$ peaks with two characteristic satellites with a

344   Fe^{2+}/Fe^{3+} ratio of 1.46:1. The high resolution Fe $2p_{3/2}$ devolution spectra show one

345   peak at 711.34 eV for divalent iron and another peak at 713.05 eV for trivalent iron

346   (Bae and Lee, 2014; Chen et al., 2018), which confirmed the presence of divalent and

347   trivalent iron in the precipitate (Fig. 5b). Divalent iron was initially derived from

348   nZVI electro-dissolution and some of the divalent iron was then further oxidized to

349   trivalent iron during the reaction. The O devolution spectra show the existence of the

18

350 peaks of –OH at 531.54 eV, lattice oxygen in metal oxides (O^{2-}) at 530.74 eV, and

351 chemically or physically adsorbed water (H_2O) at 532.91 (Fig. 5c) (Chen et al., 2018;

352 Tan et al., 2018). The ratio of H_2O : –OH : O^{2-} is 1.25 : 1.31 : 1. Nitrogen of NO_3^- is

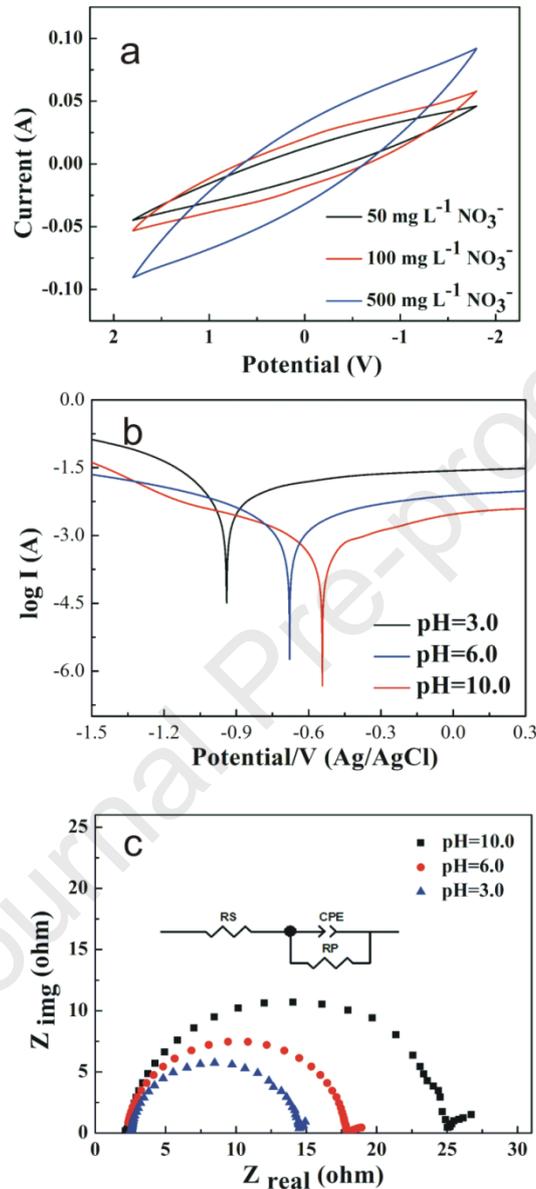353 too low to be detected by XPS in this study.

354

355 **Fig. 5** XPS spectra of the surface elements of the precipitate: a) survey spectrum; b)

356 Fe element; c) O element.

357

358 3.3 Tafel, CV, and EIS analysis

359   Tafel polarization, EIS and CV experiments were performed to gain insight into

360   the anodic reaction behaviors. Fig. 6a shows that the covered area in the CV curve

361   increases with the initial nitrate concentration while the initial pH has slight effect on

362   the CV curves (data not shown). This indicates that electric field facilitates the

363   accumulation of nitrate ions on the nZVI surface with a denser double layer and

364   further enhances the interaction between nZVI and nitrate. Fig. 6b shows the effect of

365   initial solution pH on the Tafel plots. The E_{corr} values of nZVI are -0.94 V, -0.55 V,

366   and -0.68 V at pH values of 3, 6, and 10, respectively. E_{corr} of nZVI at near neutral

367   (pH=6) has a highest value, and then E_{corr} shifts to lower potentials at either acid

368   (pH=3) or alkaline (pH=10) condition due to more vulnerable to anodic oxidation.

369   The corrosion current densities are 5.98 11.56, and 56.34 μA cm^2 at different pH

370   values (10, 6, and 3). Correspondingly, as shown in Nyquist diagram and its

371   equivalent circuit (Fig. 6c), charge-transfer resistances (R_{ct}) of the nZVI anode in

372   different pH values (10, 6, and 3) are 24.3, 17.9, and 14.6 Ω. The corresponding

373   polarization resistances (Rp) at pH of 3 has the lowest value of 12.05 Ω compared to

374   22.96 and 15.74 Ω (at pH 10 and 6), which is consistent with the observation that

375   nZVI at pH of 3 is more vulnerable to anodic oxidation. The increase in

376   charge-transfer resistances (R_{ct}) of the nZVI anode concomitant with a decrease in

377   corrosion current density along with an increase of pH value is indicative of depletion

378   of the reducible species and anodic formation of nuclei of a ferrous hydroxide film

379   responsible for the low Rct (Wang and Farrell, 2003). The degree of coverage of the

380   iron surface with the iron (hydr)oxides film is likely to increase at the more positive

20

381   potential and higher pH value because penetration of more hydroxyl ions into inner

382   part of the double layer (Foroulis, 1979).

383

384   **Fig. 6** a) Cyclic voltammetry curves for anode at the initial nitrate concentrations of

385   (50 mg L^{-1}, 100 mg L^{-1} and 500 mg L^{-1}); b) Tafel curves, c) Nyquist plot of of anode

386   at different pH values (3, 6, and 10) (Insert: The equivalent circuit).

387

388   3.4 Mechanisms of electrochemical nitrate removal

389   The schematic mechanism of the electrochemical denitrification process with

21

390 magnetically fixed nZVI anode coupled with RuO_2-IrO_2/Ti plate is shown in Fig. 7.

391 Superior reduction of nitrate with simultaneous electrochemical oxidation of

392 intermediates enhanced removal efficiency and N_2 selectivity. First, the applied

393 electric field facilitates the interaction between nZVI on anode and the negtive ion of

394 NO_3^- because more nitrate ions pile up on the nZVI surface. Second, NO_3^- is

395 simultanously reduced by the surface-adsorbed atom H* from self-produced hydrogen

396 in water electrolysis process (Zhao et al., 2022). Third, ammonia oxidation on

397 RuO_2-IrO_2/Ti plate under high voltage not only reduced the ammonia intermediates

398 and promoted the nitrate reduction reaction to the positive direction because there are

399 no obvious ammonia accumulation as shown in Fig. 3. Fouth, iron(III) hydroxide

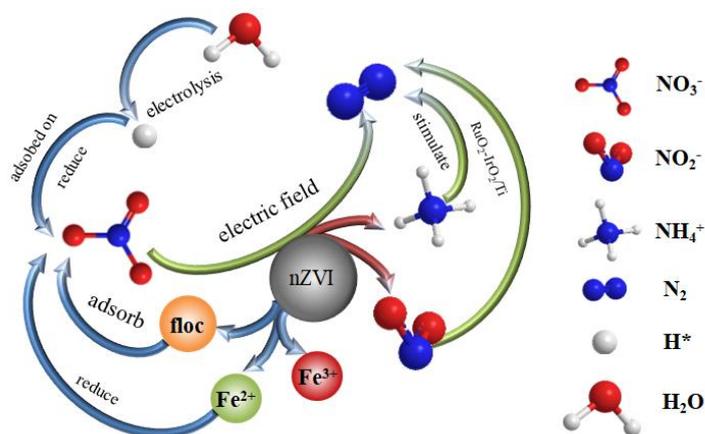400 flocs prduced in the course of nZVI coagulation also slightly contribute to the nitrate

401 removal via adsorption as shown in the xps data with nitrogen and iron elements.

402 Fifth, the presence of eletric field is also beneficial to reduce further passivation on

403 nZVI surface caused by species of iron (hydr)oxides (Luo et al., 2010). This

404 demonstrated that the coupling of RuO_2-IrO_2/Ti electrode with nZVI as an anode has

405 a significant improvement on nitrate removal and N_2 selectivity.

406

407 **Fig. 7** The schematic mechanisms of electrochemical nitrate removal.

4 Conclusions

In summary, we propose and analyze the performance of the nZVI anode based electrochemical nitrate removal process coupled with ammonia oxidation function plate (RuO$_2$-IrO$_2$/Ti). For a bulk NO$_3^-$ concentration of 100 mg L^{-1}, the maximum nitrate removal efficiency and N$_2$ selectivity reach 94.6 % and 72.8 % in 5 h, respectively. Compared to nZVI dosage, the initial pH value and the applied voltage had a strong influence on the nitrate conversion. The incorporation of RuO$_2$-IrO$_2$/Ti electrodes not only improved the nitrate conversion but also the N$_2$ selectivity because ammonia oxidation reduces the intermediates and promotes reduction reaction. The applied electric field is beneficial to the convective migration of nitrate and passivation mitigation on nZVI surface. Additionally, endogenous reactive hydrogen (atom H*) from water electrolysis process and iron hydroxides flocs from anodic oxidation enhance the nitrate removal via reduction and adsorption. CV curves confirmed the accumulation of nitrate ions on the nZVI surface with a denser double layer and further enhancement the interaction between nZVI and nitrate. Tafel polarization and EIS analysis provide the illustration that lower charge-transfer resistance (14.6 Ω) and lower corrosion potential (-0.94 V) and together with a higher corrosion current density (56.34 μA cm^2) of nZVI anode facilitates higher nitrate removal efficiency and N$_2$ selectivity. Utilization of nZVI anode coupled with ammonia oxidizing function plate can be a promising feasible approach to achieve high nitrate removal and N$_2$ selectivity.

430 **Acknowledgement**

436

437

438

439

440

441

442

443

444

445

446

447

448

449

450

451

References

Aggrwal, G., Salunke-Gawali, S.S., Gejji, S.P., Nikalje, M., Chakravarty, D., Verma, P.L., Gosavi-Mirkute, P.G., Harihar, S., Jadhav, M., Puranik, V.G., 2021. Reactions of 2,3-dibromonaphthalene-1,4-dione and pyridyl amines: X-ray Structures, DFT investigations, and selective detection of the Hg^{2+} and Ni^{2+} ions. Eng. Sci. 14, 78-93.

Alowitz, M.J., Scherer, M.M., 2002. Kinetics of nitrate, nitrite, and Cr(VI) reduction by iron metal. Environ. Sci. Technol. 36, 299-306.

Amarine, M., Lekhlif, B., Sinan, M., El Rharras, A., Echaabi, J., 2020. Treatment of nitrate-rich groundwater using electrocoagulation with aluminum anodes. Groundw. Sustain. Dev. 11, 100371.

Bae, S., Lee, W., 2014. Influence of riboflavin on nanoscale zero-valent iron reactivity during the degradation of carbon tetrachloride. Environ. Sci. Technol. 48, 2368-2376.

Benekos, A.K., Tziora, F.E., Tekerlekopoulou, A.G., Pavlou, S., Qun, Y., Katsaounis, A., Vayenas, D.V., 2021. Nitrate removal from groundwater using a batch and continuous flow hybrid Fe-electrocoagulation and electrooxidation system. J. Environ. Manage. 297, 113387.

Chauhan, R., Srivastava, V.C., 2020. Electrochemical denitrification of highly contaminated actual nitrate wastewater by Ti/RuO_2 anode and iron cathode. Chem. Eng. J. 386, 122065.

Chen, W., Zhang, A., Gu, Z., Li, Q., 2018. Enhanced degradation of refractory organics in concentrated landfill leachate by Fe^0/H_2O_2 coupled with microwave irradiation. Chem. Eng. J. 354, 680-691.

474 Fan, T., Deng, W., Gang, Y., Du, Z., Li, Y., 2021. Degradation of hazardous organics

475 via cathodic flow-through process using a spinel $FeCo_2O_4$/CNT decorated

476 stainless-steel mesh. ES Mater. Manuf. 12, 53-62.

477 Foroulis, Z.A., 1979. The kinetics of anodic dissolution of iron in high purity water.

478 Corrosion Engineering 28, 10-17.

479 Guo, W., Zhao, Q., Du, J., Wang, H., Li, X., Ren, N., 2020. Enhanced removal of

480 sulfadiazine by sulfidated ZVI activated persulfate process: performance, mechanisms

481 and degradation pathways. Chem. Eng. J. 388, 124303.

482 Huang, X., Zhang, F., Peng, K., Liu, J., Lu, L., Li, S., 2020. Effect and mechanism of

483 graphene structured palladized zero-valent iron nanocomposite (nZVI-Pd/NG) for

484 water denitration. Sci. Rep. 10, 9931.

485 Huang, Y.H., Zhang, T.C., 2005. Effects of dissolved oxygen on formation of

486 corrosion products and concomitant oxygen and nitrate reduction in zero-valent iron

487 systems with or without aqueous Fe^{2+}. Water Res. 39, 1751-1760.

488 Jiang, Z., Zhang, S., Pan, B., Wang, W., Wang, X., Lv, L., Zhang, W., Zhang, Q., 2012.

489 A fabrication strategy for nanosized zero valent iron (nZVI)–polymeric anion

490 exchanger composites with tunable structure for nitrate reduction. J. Hazard. Mater.

491 233-234, 1-6.

492 Katsounaros, I., Kyriacou, G., 2007. Influence of the concentration and the nature of

493 the supporting electrolyte on the electrochemical reduction of nitrate on tin cathode.

494 Electrochim. Acta 52, 6412-6420.

495 Khalil, A.M.E., Eljamal, O., Saha, B.B., Matsunaga, N., 2018. Performance of

496 nanoscale zero-valent iron in nitrate reduction from water using a laboratory-scale

497 continuous-flow system. Chemosphere 197, 502-512.

498 Li, L., Zhou, Y., Zhang, Y., Huang, Y., Goel, R., 2016. Enhanced electrolytic nitrate

499 reduction utilizing a three-dimensional electrolysis reactor packed with activated

500 carbon and foamed copper. Environ. Eng. Sci. 33, 525-535.

501 Li, X., Yan, J., Zhu, K., 2021. Fabrication and characterization of Pt doped

502 Ti/Sb-SnO$_2$ electrode and its efficient electro-catalytic activity toward phenol. Eng.

503 Sci. 15, 38-46.

504 Liu, Y., Liu, S., Yang, Z., Xiao, L., 2021. Synergetic effects of biochars and denitrifier

505 on nitrate removal. Bioresour. Technol. 335, 125245.

506 Liu, Y., Wang, J., 2019. Reduction of nitrate by zero valent iron (ZVI)-based materials:

507 A review. Sci. Total Environ. 671, 388-403.

508 Luo, H., Jin, S., Fallgren, P.H., Colberg, P.J.S., Johnson, P.A., 2010. Prevention of

509 iron passivation and enhancement of nitrate reduction by electron supplementation.

510 Chem. Eng. J. 160, 185-189.

511 Ma, Z., Klimpel, M., Budnyk, S., Rokicińska, A., Kuśtrowski, P., Dronskowski, R.,

512 Mathew, A.P., Budnyak, T., Slabon, A., 2021. Combining Electrocatalysts and

513 Biobased Adsorbents for Sustainable Denitrification. ACS Sustain. Chem. Eng. 9,

514 3658-3667.

515 Pang, Y., Wang, J., 2021. Various electron donors for biological nitrate removal: A

516 review. Sci. Total Environ. 794, 148699.

517 Pellessier, J., Gang, Y., Li, Y., 2021. A sustainable synthesis of nickel-nitrogen-carbon

27

518 catalysts for efficient electrochemical CO_2 reduction to CO. ES Mater. Manuf. 13,

519 66-75.

520 Puggioni, G., Milia, S., Dessì, E., Unali, V., Pous, N., Balaguer, M.D., Puig, S.,

521 Carucci, A., 2021. Combining electro-bioremediation of nitrate in saline groundwater

522 with concomitant chlorine production. Water Res. 206, 117736.

523 Qi, G., Liu, Y., Chen, L., Xie, P., Pan, D., Shi, Z., Quan, B., Zhong, Y., Liu, C., Fan,

524 R., Guo, Z., 2021. Lightweight $Fe_3C@Fe/C$ nanocomposites derived from wasted

525 cornstalks with high-efficiency microwave absorption and ultrathin thickness. Adv.

526 Compos. Hybrid Mater. 4, 1226-1238.

527 Ramalingam, S., Subramania, A., 2021. Effective removal of nitrates from the

528 drinking water by chemical and electrochemical methods. Eng. Sci. 15, 80-88.

529 Salam, M.A., Fageeh, O., Al-Thabaiti, S.A., Obaid, A.Y., 2015. Removal of nitrate

530 ions from aqueous solution using zero-valent iron nanoparticles supported on high

531 surface area nanographenes. J. Mol. Liq. 212, 708-715.

532 Singh, S., Anil, A.G., Kumar, V., Kapoor, D., Subramanian, S., Singh, J., Ramamurthy,

533 P.C., 2022. Nitrates in the environment: A critical review of their distribution, sensing

534 techniques, ecological effects and remediation. Chemosphere 287, 131996.

535 Song, N., Chen, Z., Shi, J., Shi, D., Gu, L., 2021. Performance and mechanism of

536 chelating resin (TP-207) supported Pd/Cu bimetallic nanoparticles in selective

537 reduction of nitrate by using ZVI (zero valent iron) as reductant. Sep. Purif. Technol.

538 272, 118974.

539 Su, L., Han, D., Zhu, G., Xu, H., Luo, W., Wang, L., Jiang, W., Dong, A., Yang, J.,

540   2019. Tailoring the assembly of iron nanoparticles in carbon microspheres toward

541   high-performance electrocatalytic denitrification. Nano Lett. 19, 5423-5430.

542   Su, Y., Adeleye, A.S., Huang, Y., Sun, X., Dai, C., Zhou, X., Zhang, Y., Keller, A.A.,

543   2014. Simultaneous removal of cadmium and nitrate in aqueous media by nanoscale

544   zerovalent iron (nZVI) and Au doped nZVI particles. Water Res. 63, 102-111.

545   Sun, D., Hong, X., Wu, K., Hui, K.S., Du, Y., Hui, K.N., 2020. Simultaneous removal

546   of ammonia and phosphate by electro-oxidation and electrocoagulation using

547   RuO_2-IrO_2/Ti and microscale zero-valent iron composite electrode. Water Res. 169,

548   115239.

549   Tan, C., Dong, Y., Fu, D., Gao, N., Ma, J., Liu, X., 2018. Chloramphenicol removal

550   by zero valent iron activated peroxymonosulfate system: kinetics and mechanism of

551   radical generation. Chem. Eng. J. 334, 1006-1015.

552   Teng, W., Bai, N., Liu, Y., Liu, Y., Fan, J., Zhang, W.-x., 2018. Selective nitrate

553   reduction to dinitrogen by electrocatalysis on nanoscale iron encapsulated in

554   mesoporous carbon. Environ. Sci. Technol. 52, 230-236.

555   Wang, J., Deng, Z., Feng, T., Fan, J., Zhang, W.-x., 2021a. Nanoscale zero-valent iron

556   (nZVI) encapsulated within tubular nitride carbon for highly selective and stable

557   electrocatalytic denitrification. Chem. Eng. J. 417, 129160.

558   Wang, J., Farrell, J., 2003. Investigating the role of atomic hydrogen on chloroethene

559   reactions with iron using Tafel analysis and electrochemical impedance spectroscopy.

560   Environ. Sci. Technol. 37, 3891-3896.

561   Wang, Z., Chen, G., Wang, X., Yang, G., Liu, Y., Zhang, C., 2021b. Performance of

562 L-Cu&Mn-nZVFe@B nanomaterial on nitrate selective reduction under UV

563 irradiation and persulfate activation in the presence of oxalic acid. J. Hazard. Mater.

564 401, 123378.

565 Wei, A., Ma, J., Chen, J., Zhang, Y., Song, J., Yu, X., 2018. Enhanced nitrate removal

566 and high selectivity towards dinitrogen for groundwater remediation using

567 biochar-supported nano zero-valent iron. Chem. Eng. J. 353, 595-605.

568 Wu, H., Zhong, Y., Tang, Y., Huang, Y., Liu, G., Sun, W., Xie, P., Pan, D., Liu, C.,

569 Guo, Z., 2021. Precise regulation of weakly negative permittivity in $CaCu_3Ti_4O_{12}$

570 metacomposites by synergistic effects of carbon nanotubes and grapheme. Adv.

571 Compos. Hybrid Mater. https://doi.org/10.1007/s42114-021-00378-y

572 Yang, Z., Shan, C., Mei, Y., Jiang, Z., Guan, X., Pan, B., 2018. Improving reductive

573 performance of zero valent iron by H_2O_2/HCl pretreatment: A case study on nitrate

574 reduction. Chem. Eng. J. 334, 2255-2263.

575 Zhang, Y., Douglas, G.B., Pu, L., Zhao, Q., Tang, Y., Xu, W., Luo, B., Hong, W., Cui,

576 L., Ye, Z., 2017. Zero-valent iron-facilitated reduction of nitrate: Chemical kinetics

577 and reaction pathways. Sci. Total Environ. 598, 1140-1150.

578 Zhang, Y., Zhao, Y., Chen, Z., Wang, L., Wu, P., Wang, F., 2018. Electrochemical

579 reduction of nitrate via Cu/Ni composite cathode paired with Ir-Ru/Ti anode: High

580 efficiency and N_2 selectivity. Electrochim. Acta 291, 151-160.

581 Zhao, F., Xin, J., Yuan, M., Wang, L., Wang, X., 2022. A critical review of existing

582 mechanisms and strategies to enhance N_2 selectivity in groundwater nitrate reduction.

583 Water Res. 209, 117889.

Highlights:

►Electrochemical nitrate removal was performed on nZVI/RuO_2-IrO_2/Ti anode.

►High nitrate removal efficiency and nitrogen selectivity was achieved near neutral medium.

►Electro-denitrification activity and N_2 selectivity was evaluated under different parameters.

►The mechanisms were proposed based on physiochemical and electrochemical properties of anode.

Declaration of interests

☒ The authors declare that they have no known competing financial interests or personal relationships that could have appeared to influence the work reported in this paper.

☐The authors declare the following financial interests/personal relationships which may be considered as potential competing interests: